OXFORD

JNCI J Natl Cancer Inst (2018) 110(3): djx198

doi: 10.1093/jnci/djx198
First published online September 27, 2017
Article

ARTICLE

Nicotinamide Phosphoribosyltransferase (NAMPT) as a Therapeutic Target in BRAF-Mutated Metastatic Melanoma

Valentina Audrito, Antonella Managò, Sofia La Vecchia, Federica Zamporlini, Nicoletta Vitale, Gianna Baroni, Simona Cignetto, Sara Serra, Cinzia Bologna, Aureliano Stingi, Francesca Arruga, Tiziana Vaisitti, Daniela Massi, Mario Mandalà, Nadia Raffaelli, Silvia Deaglio

Affiliations of authors: Department of Medical Sciences (VA, AM, SLV, SC, SS, CB, AS, FA, TV, SD) and Department of Molecular Biotechnologies and Health Science (NV), University of Turin, Italy; Italian Institute for Genomic Medicine, Turin, Italy (VA, AM, SLV, SC, SS, CB, AS, FA, TV, SD); Department of Agricultural, Food and Environmental Sciences, Polytechnic University of Marche, Ancona, Italy (FZ, NR); Division of Pathological Anatomy, Department of Surgery and Translational Medicine, University of Florence, Italy (GB, DM); Unit of Medical Oncology, Department of Oncology and Hematology, Papa Giovanni XXIII Hospital, Bergamo, Italy (MM).

Correspondence to: Silvia Deaglio, MD, PhD, Department of Medical Sciences, University of Turin School of Medicine and Italian Institute for Genomic Medicine (IIGM, formerly HuGeF), via Nizza, 52, 10126 Torino, Italy (e-mail: silvia.deaglio@unito.it or silvia.deaglio@iigm.it).

Abstract

Background: One of the effects of oncogenic signaling is metabolic reprogramming of tumor cells to support anabolic growth, opening the way to therapeutic targeting of metabolic pathways.
Methods: We studied NAD biosynthesis in BRAF inhibitor (BRAFi)–resistant (BiR) melanoma cell lines. Data in cell lines were confirmed by immunohistochemistry in biopsies from 17 patients with metastatic melanoma (MM) before and after the acquisition of resistance to BRAFi. Therapeutic potential of NAD biosynthesis inhibitors was determined by in vitro monitoring cell growth and death and in mouse xenograft models. Mice (n = 6–10 mice/group) were treated with nicotinamide phosphoribosyltranferase inhibitor (NAMPTi), BRAFi, or their combination, and tumor growth and survival were analyzed. All statistical tests were two-sided.
Results: BiR cells had higher NAD levels compared with their BRAFi-sensitive counterparts ($P < .001$ and $P = .001$ for M14 and A375, respectively) and with normal melanocytes ($P < .001$), achieved through transcriptional upregulation of the enzyme NAMPT, which became the master regulator of NAD synthesis. Conversely, treatment with BRAFi or MEK inhibitors decreased NAMPT expression and cellular NAD levels. Robust NAMPT upregulation was documented in tissue biopsies from MM patients after development of resistance to BRAFi ($P < .001$). Treatment of melanoma cells with NAMPTi depleted NAD and ATP, depolarized mitochondrial membrane, and led to reactive oxygen species production, blocking cells in the G2/M phase and inducing apoptosis. Treatment of BiR xenografts with NAMPTi improved mouse survival (median survival of vehicle-treated mice was 52 days vs 100 days for NAMPTi-treated ones in M14/BiR, while in A375/BiR median survival of vehicle-treated mice was 23.5 days vs 43 days for NAMPTi-treated ones, $P < .001$).
Conclusions: BiR melanoma cells overexpress NAMPT, which acts as a connecting element between BRAF oncogenic signaling and metabolism, becoming an actionable target for this subset of MM patients.

Received: February 22, 2017; **Revised:** June 16, 2017; **Accepted:** August 15, 2017

Nicotinamide adenine dinucleotide (NAD) is a key element in both energy production and signal transduction pathways (1,2). By acting as a cofactor for enzymes involved in energy metabolism, NAD facilitates electron transfer in central metabolic processes (3). Additionally, it can also serve as substrate for different classes of enzymes, including sirtuins and poly ADP-ribose polymerases, involved in the regulation of metabolic checkpoints, DNA repair, inflammation, and protein acetylation, among other physiological processes (3). Because these enzymes consume NAD, cells need to incessantly regenerate it. Nicotinamide phosphoribosyltransferase (NAMPT, also known as pre-B colony enhancing factor [PBEF] or visfatin), is the rate-limiting enzyme involved in the conversion of nicotinamide to NAD (4,5). NAMPT is frequently upregulated in hematological malignances and in solid tumors, including melanoma (5–7). Two NAMPT inhibitors (NAMPTi), FK866 and GMX1778, have demonstrated potent anticancer activity in preclinical tumor models (8,9) by depleting NAD levels and blocking tumor growth (10,11).

The working hypothesis behind this paper is that oncogenic signaling directly affects NAMPT-controlled NAD biosynthesis. To test this hypothesis, we selected BRAF-mutated metastatic melanomas (MM) carrying the V600E activating mutation in the BRAF oncogene (12,13). These tumors, approximately 40% to 50% of metastatic melanomas, are uniquely sensitive to BRAF inhibitors (BRAFi), vemurafenib and dabrafenib. However, MM patients treated with BRAFi invariably develop resistance, characterized by the reactivation of the MAPK pathway (14–17) and metabolic adaptation through either enhanced mitochondrial respiration or glycolysis (18–21).

In the present study, we observed that BRAFi-resistant cells (BiR) contain higher NAD levels, obtained through the selective upregulation of NAMPT. Consequently, we tested the hypothesis that NAMPT is an actionable target for this subset of melanoma patients.

Methods

A complete description of the methods can be found in the Supplementary Methods (available online).

Patients and Cells

Patient material was collected after obtaining written informed consent and in accordance with the Institutional Review Board and the Declaration of Helsinki. M14 and A375 $BRAF^{V600E}$-mutated cell lines were from the American Type Culture Collection (ATCC). BRAFi-resistant variants were generated by culturing cells with increasing concentrations of the BRAF inhibitor dabrafenib (GlaxoSmithKline, Brentford, UK), reaching the concentration of 1.6 μM in approximately 10 to 12 weeks and maintained thereafter. Adult epidermal melanocytes were from Thermo Fisher Scientific (Monza, Italy).

Seahorse Metabolic Experiments

Real-time measurements of oxygen consumption rate (OCR) and extracellular acidification rate (ECAR) were made using an XFp Extracellular Flux Analyzer (Agilent Technologies, Santa Clara, CA). Full details are in the Supplementary Methods (available online).

NAD and ATP Determination

NAD and ATP were extracted from cells and tissues as described in Mori et al. (22) and quantified by UV C18-HPLC analysis under ion-pairing conditions.

NAMPT Overexpression

NAMPT overexpression was obtained by transducing sensitive (S) M14 and A375 cells with a lentiviral vector carrying NAMPT-GFP-tag or with the GFP-tag alone. GFP^+ cells were flow sorted (FACSAriaIII, BD Bioscience, Milan, Italy) and used for further experiments. Full details are provided in the Supplementary Methods (available online).

Xenograft Models

Melanoma cells (5×10^6, in Matrigel, Corning, Corning, NY) were injected subcutaneously in eight-week-old male NOD/SCID/γOD/$SC^{-/-}$ (NSG) mice. All mice were bred at the Animal Facility of the Molecular Biotechnology Center (Torino, Italy), recognized and approved by the Italian Ministry of Health.

When tumors became palpable, mice (n = 6–10 mice per group) were treated as indicated in the Supplementary Methods (available online).

Statistical Analyses

Statistical analyses were performed with GraphPad version 6.0 (GraphPad Software Inc., La Jolla, CA). Continuous variables were analyzed by Mann–Whitney U (unpaired data), and paired t test or Wilcoxon signed rank (paired data) tests. Matched groups (three or more) were compared using one-way analysis of variance with Dunn's multiple comparisons.

Results are reported as box plots, where the top and bottom margins of the box define the 25th and 75th percentiles, the line in the box defines the median, and the error bars define the minimum and maximum of all data. Survival curves were estimated with the Kaplan-Meier method. The log-rank test was used for statistical analysis. A P value of less than .05 was considered to be statistically significant. All statistical tests were two-sided.

Results

Metabolic Adaptation Mechanisms in BRAFi-Resistant Melanoma Cells

To study NAD biosynthesis after metabolic adaptation of melanoma cells, we selected $BRAF^{V600E}$-mutated cell lines and made them resistant to BRAFi (A375/BiR and M14/BiR). As expected (17,23), BiR cells were insensitive to BRAFi (Figure 1A) and showed constitutive activation of the MAPK axis, downstream of BRAF (Supplementary Figure 1, available online). Furthermore, wound-healing experiments confirmed that BiR cells were more aggressive than S cells ($P = .007$ and $P < .001$ for M14 and A375, respectively) (Figure 1B), as also demonstrated after measuring growth in NSG mice ($P < .001$ for both lines) (Figure 1C).

Development of BRAFi resistance was accompanied by metabolic adaptation. Analysis of ECAR and OCR, indicators of aerobic glycolysis and OXPHOS, respectively, showed increased steady state and maximal glycolysis and respiration in BiR

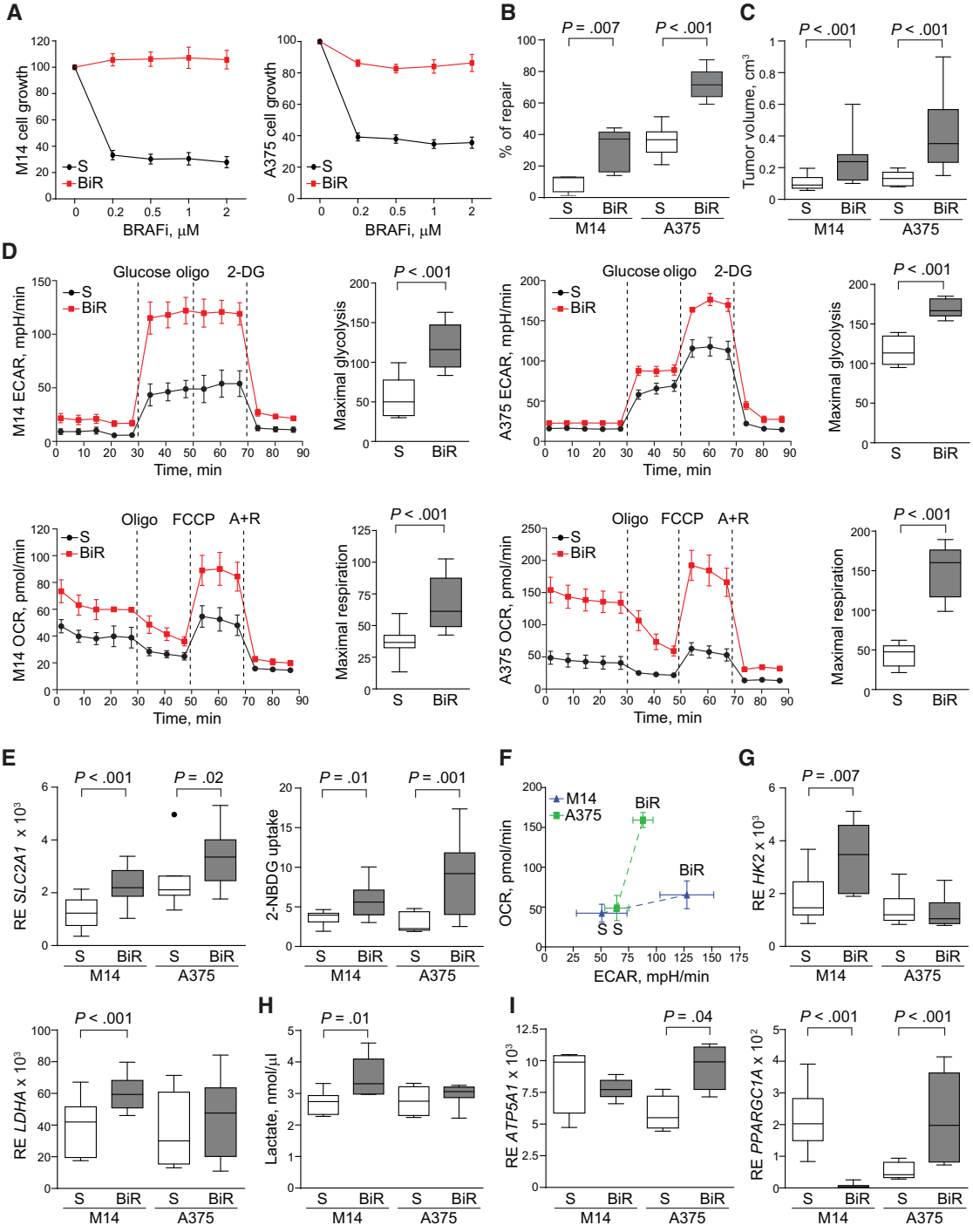

Figure 1. Different pathways of metabolic adaptation in M14/BiR and A375/BiR cells. **A)** Cell growth of M14 and A375 melanoma cell lines sensitive (S, **black line**) or resistant (BiR, **red line**) to BRAFi (dabrafenib) used at scalar doses for 72 hours as measured by MTT assay. Data are represented as percentage of control (untreated cells). Data from five independent experiments, each performed in triplicate. **B)** Box plot shows percentage of wound healing repair, calculated as [(area 24 hours/area 0 hours) × 100]. Data from six independent experiments. **C)** Box plot shows tumor volume in NOD/SCID/γchain$^{-/-}$ mice xenografted with M14/S or /BiR and A375/S or /BiR variants (5×10^6 cells, injected subcutaneously) and evaluated after 30 days. At least 10 mice under each condition were evaluated. **D)** Extracellular acidification rate (ECAR) and steady-state O_2 consumption rate (OCR) measured in M14/S and /BiR and A375/S and /BiR variants using the Seahorse XFp Analyzer. Box plots represent cumulative data of maximal glycolysis (ECAR values after oligomycin injection) and maximal respiration calculated as: (OCR after FCCP – OCR after antimycin+rotenone addition). **E)** Box plots reporting mRNA expression levels of the glucose transporter GLUT1/*SLC2A1* and glucose internalization, analyzed as mean fluorescence intensity of cells incubated (10 minutes, 37 °C) with the fluorescent deoxyglucose analog 2-NBDG. **F)** Plot showing the metabolic shift occurring as a consequence of the transition from the S to the BiR phenotype in M14 and A375 variants. Data are plotted as OCR (pmol/min, y-axis) vs ECAR (mpH/min, x-axis). **G)** Quantitative real-time polymerase chain reaction (qRT-PCR) analysis of the expression of the glycolytic enzymes *HK2* and *LDHA*. **H)** Lactate levels (nmol/mL measured in supernatants from M14/S and /BiR and A375/S and /BiR cell cultures. **I)** qRT-PCR analysis showing expression of *ATP5A1* and *PPARGC1A*. In all qRT-PCR experiments, expression levels of the analyzed gene were normalized over actin. Results were obtained from at least six independent experiments, each performed in triplicate. All statistical analyses were performed using two-sided Mann–Whitney U test. **Boxes** represent interquartile range, and the **horizontal line across each box** indicates the median. 2-DG = 2-Deoxy-D-glucose; A+R = antimycin+rotenone; BiR = BRAFi-resistant; ECAR = extracellular acidification rate; FCCP = carbonyl cyanide p-trifluoromethoxyphenylhydrazone; Oligo = oligomycin; S = BRAFi-sensitive.

ARTICLE

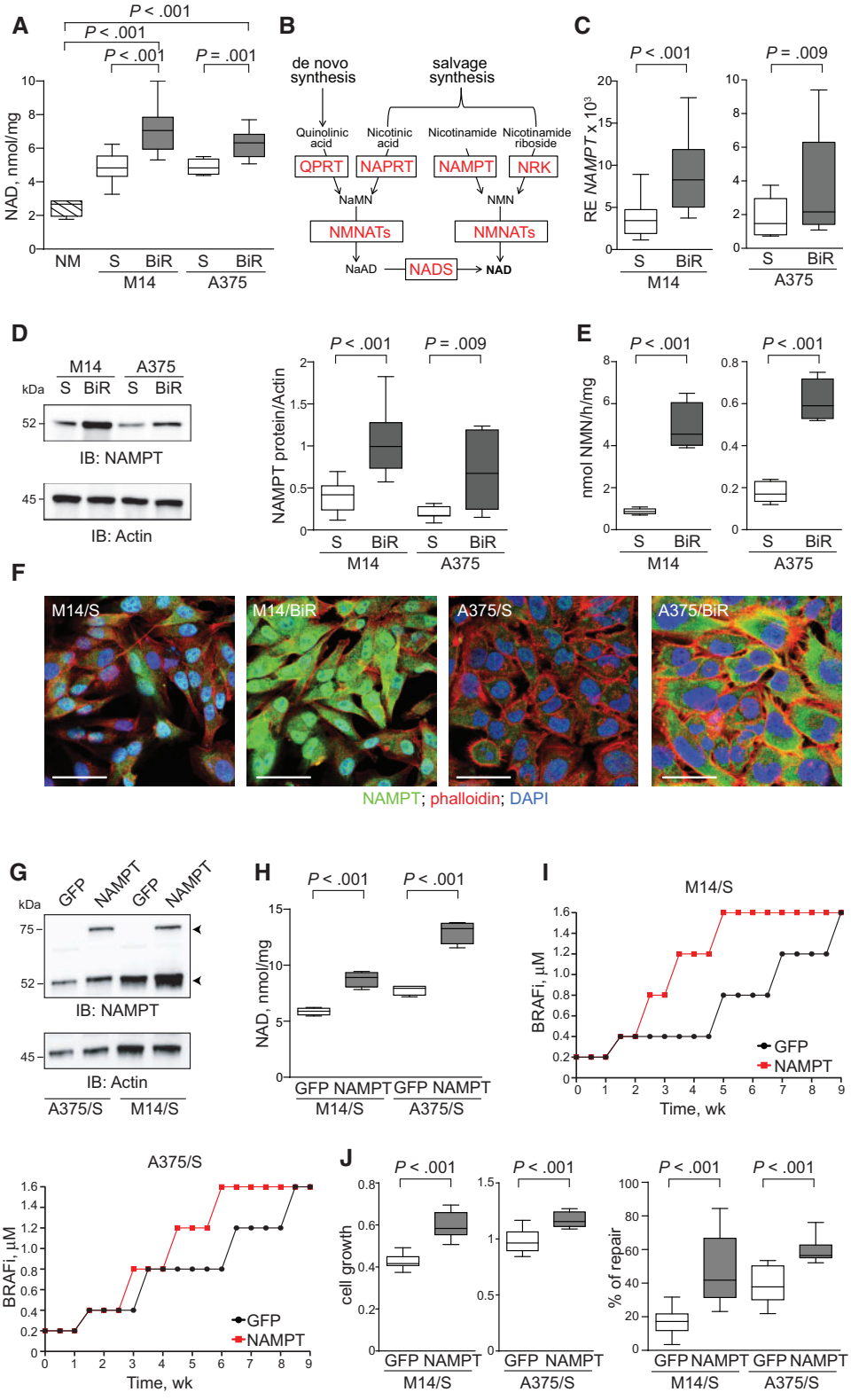

Figure 2. NAD biosynthetic pathways in BRAFi-resistant (BiR) cells. **A)** Box plots representing NAD intracellular concentrations (nmol/mg proteins) measured from extracts of the indicated cells. **B)** Schematic representation of NAD biosynthetic pathways in mammalian cells. **C)** Box plots reporting *NAMPT* mRNA expression levels in BRAFi-sensitive (S) and BiR cells. **D)** Analysis of NAMPT expression in M14/S and /BiR and A375/S and /BiR variants by immunoblot. Box plots show cumulative data of band quantification (n = 5) represented as ratio of the enzyme/actin levels. **E)** Box plots representing NAMPT enzymatic activity expressed as nmol NMN/h/mg measured simultaneously in cell extracts from the indicated cell lines using fluorometric assays. **F)** NAMPT expression evaluated by confocal immunofluorescence staining (original magnification 63×) in S and BiR cells. **Scale bar** = 50 µm. **G)** NAMPT expression evaluated by immunoblot in S cells infected with a lentivirus carrying a NAMPT-GFP (indicated as NAMPT) or a GFP-only (indicated as GFP) constructs. **Arrows** show endogenous NAMPT (**lower bands**) and fused protein GFP-NAMPT

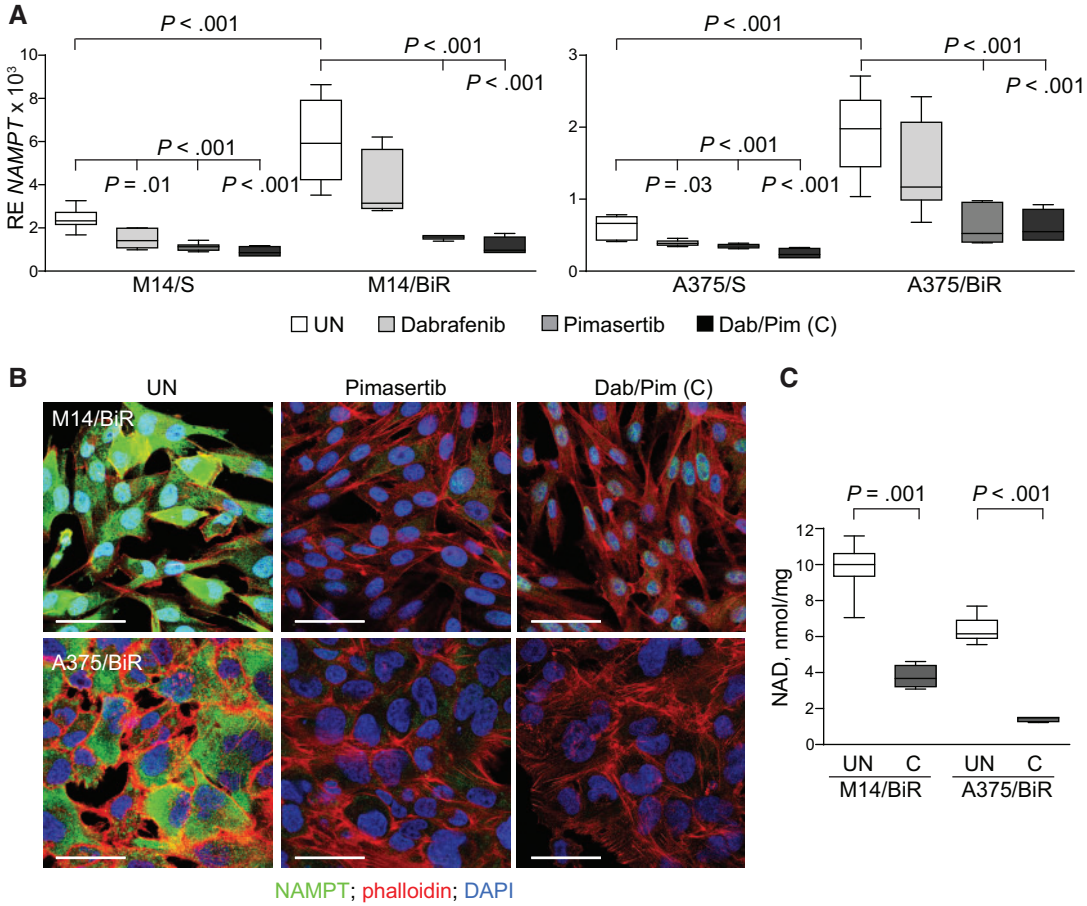

Figure 3. Effects of MAPK inhibitors on NAMPT expression and NAD production. **A)** Box plots reporting *NAMPT* mRNA expression levels in the untreated condition (UN), or after 24 hours of treatment with the BRAFi dabrafenib, the MEK inhibitor pimasertib (both used at 5 μM), or their combination (indicated as Dab/Pim, C). Data from seven experiments. Statistical analysis was performed using two-sided multiple-comparisons and Mann–Whitney U tests. **Boxes** represent interquartile range, and the **horizontal line across each box** indicates the median. **B)** Confocal microscopy analysis of NAMPT expression in BiR cells (**green fluorescence**) upon treatment with the indicated inhibitors. Original magnification 63×. **Scale bar** = 50 μm. Representative images from three experiments. **C)** Box plots representing intracellular NAD concentrations (nmol/mg proteins), as measured from extracts of the BiR cells upon Dab/Pim **(C)** treatments. Data from four experiments. Two-sided paired Student's *t* test was used to determine statistical significance. **Boxes** represent interquartile range, and the **horizontal line across each box** indicates the median. BiR = BRAFi-resistant; C = combination; S = BRAFi-sensitive; UN = untreated condition.

compared with S cells ($P < .001$) (Figure 1D; Supplementary Figure 2A, available online). Both BiR cell lines upregulated the glucose transporter GLUT1/*SLC2A1* and internalized glucose in a more efficient way than S cells (Figure 1E). However, while A375/BiR relied predominantly on OXPHOS, M14/BiR shifted toward a glycolytic-Warburg phenotype (Figure 1F). In fact, M14/BiR increased expression of hexokinase 2 (*HK2*), lactate dehydrogenase A (*LDHA*) (Figure 1G), pyruvate kinase isozyme M2 (*PKM2*), and enolase 1 (*ENO1*) (Supplementary Figure 2B, available online) in a statistically significant way compared with the counterparts. Accordingly, M14/BiR exported higher levels of lactate in the supernatant than M14/S cells ($P = .01$) (Figure 1H), likely due to increased expression of the lactate transporter MCT4/*SLC16A3* (Supplementary Figure 2C, available online). On the contrary, A375/BiR showed a statistically significant increase in the expression of ATP synthase subunit alpha (*ATP5A1*) and superoxide dismutase 2 (*SOD2*), both critical to oxidative metabolism (Figure 1I; Supplementary Figure 2D, available online), without modulation of glycolytic enzymes. Peroxisome proliferator-activated receptor gamma coactivator 1-alpha (PGC-1α/*PPARGC1A*), which regulates mitochondrial metabolism and is connected to oncogenic BRAF signaling (24–26),

Figure 2. Continued
(**upper bands**). **H)** Box plots representing NAD intracellular concentrations (nmol/mg proteins) measured from extracts of the indicated cells. **I)** Cell growth kinetics of M14/S-GFP and A375/S-GFP (**black lines**) and M14/S-NAMPT and A375/S-NAMPT (**red lines**) to BRAFi (dabrafenib) used at increasing concentrations (from 0.2 μM to 1.6 μM) to generate BRAFi resistance. **J)** Basal cell growth of NAMPT overexpressing vs control GFP cells, as measured by the MTT assay. Data are from nine independent experiments (each performed in triplicate) and are represented as absorbance 595 nm arbitrary unit (a.u.). On the **right**, box plot shows % of wound healing repair, calculated as [(area 24 hours/area 0 hours) × 100]. Data are from six independent experiments. All statistical analyses were performed using two-sided Mann–Whitney U test. **Boxes** represent interquartile range, and the **horizontal line across each box** indicates the median. BiR = BRAFi-resistant; NaAD = nicotinic acid adenine dinucleotide; NADS = nicotinamide adenine dinucleotide synthase; NaMN = nicotinic acid mononucleotide; NAMPT = nicotinamide phosphoribosyltransferase; NAPRT = nicotinic acid phosphoribosyltransferase; NMN = nicotinamide mononucleotide; NMNATs = nicotinamide mononucleotide adenylyltransferases; NRK = nicotinamide riboside kinase; QPRT = quinolinate phosphoribosyltransferase; S = BRAFi-sensitive.

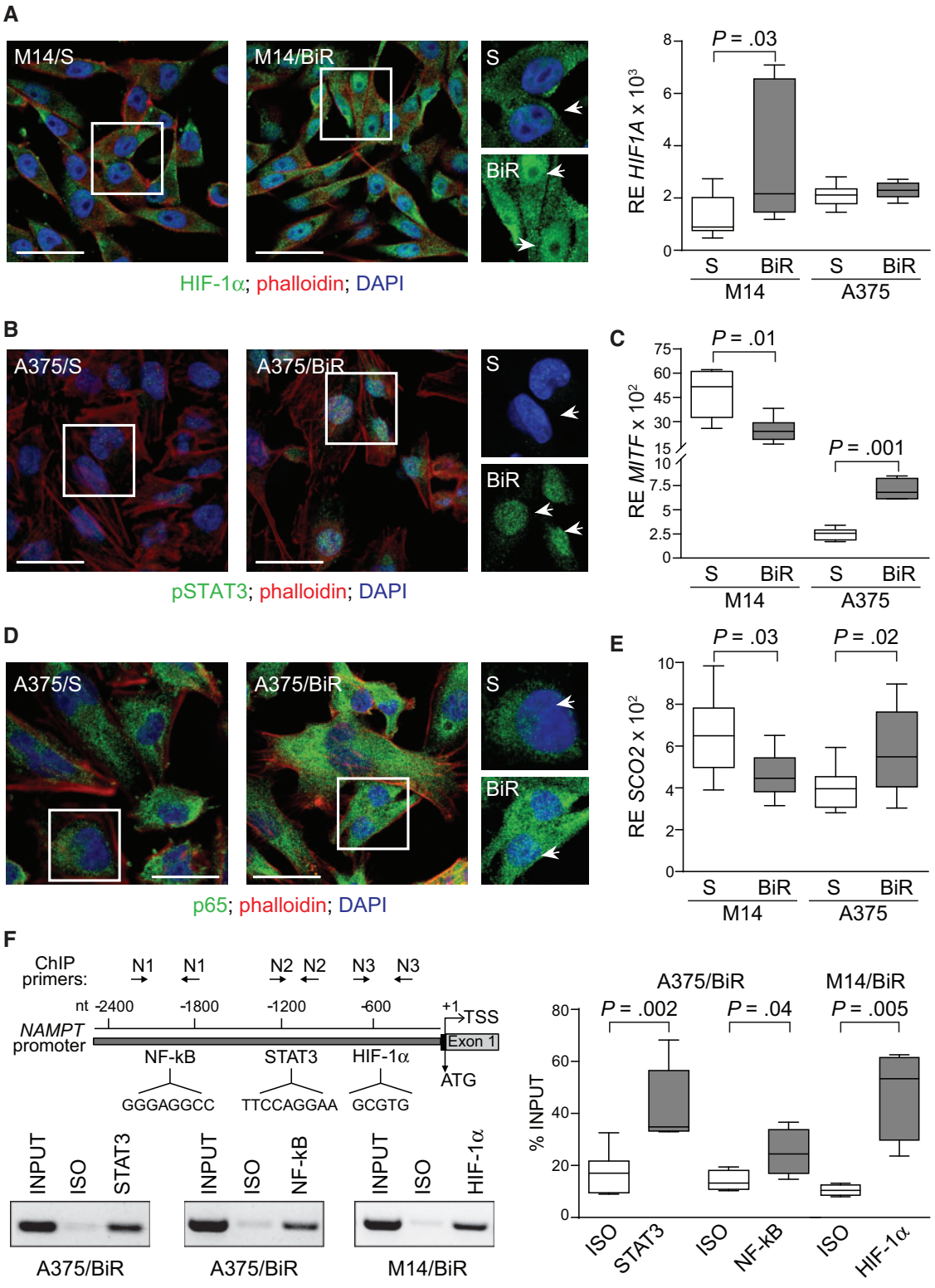

Figure 4. HIF-1α, STAT3, and NF-kB activate *NAMPT* transcription in BRAFi-resist (BiR) cells. **A)** Confocal microscopy analysis of HIF-1α expression in M14/S and /BiR (**green fluorescence**) showing increased localization of HIF-1α in the nucleus in the M14/BiR variant compared with the M14/S. Original magnification 63×. **Scale bar** = 50 μm. The **small squares** represent the zoomed area defined by the **white perimeter**. On the **right**, quantitative real-time polymerase chain reaction (qRT-PCR) analysis of the expression of *HIF1A* in the indicated cell lines. **B)** Immunofluorescence staining of the transcription factor STAT3 (**green**, 63× original magnification, **scale bar** = 50 μm), demonstrating constitutive phosphorylation in A375/BiR. The **small squares** represent the zoomed area defined by the **white perimeter**. **C)** Box plot showing mRNA expression levels of the transcription factor *MITF* in the indicated cell lines. **D)** Confocal microscopy analysis of p65 (**green**) expression in A375/S and /BiR cells, clearly showing nuclear localization in A375/BiR; 63× original magnification. **Scale bar** = 50 μm. The **small squares** represent the zoomed area defined by the **white perimeter**. **E)** Box plot on the **right** shows mRNA expression level of *SCO2*. In qRT-PCR experiments, expression levels of the analyzed gene were normalized over actin.

increased only in A375/BiR cells, confirming their reliance on OXPHOS (Figure 1I).

NAD Generation Pathways in BiR Cells

Independently of metabolic adaptation, BiR cells were characterized by markedly higher NAD levels compared with S cells (mean = 4.8 ± 0.9 in S vs 7.2 ± 1.4 nmol/mg in BiR cells for M14, $P < .001$; mean = 4.9 ± 0.4 in S vs 6.3 ± 0.8 nmol/mg in BiR cells for A375, $P = .001$), and even more so compared with normal melanocytes (mean = 2.5 ± 0.5 nmol/mg, $P < .001$) (Figure 2A), prompting the question of which NAD biosynthetic pathway is upregulated in BiR cells. NAD may be synthesized through one de novo and three salvage pathways, each controlled by a rate-limiting enzyme (Figure 2B) (27). We found that *NAMPT* was selectively upregulated in both BiR cell lines ($P < .001$ and $P = .009$ and for M14 and A375, respectively) (Figure 2C). The genes coding for the other rate-limiting NAD biosynthetic enzymes (NBEs), that is, *NAPRT*, *NMRK1*, and *QPRT*, were either downmodulated or not modified (Supplementary Figure 3A, available online). At the protein level, immunoblot and confocal microscopy confirmed selective and robust upregulation of NAMPT in both BiR lines (Figure 2, D–F; Supplementary Figure 3, B and C, available online).

Furthermore, NAMPT activity markedly increased in both BiR cell lines ($P < .001$) (Figure 2E) (28), while NRK and QPRT remained unchanged in BiR cells and NAPRT was moderately increased in M14/BiR, but not in A375/BiR cells (Supplementary Figure 3D, available online).

These findings imply that NAMPT becomes the master regulator of NAD synthesis in M14/BiR and A375/BiR, even if these cells adapt differently to oncogenic signaling. We then stably overexpressed NAMPT in S cells (Figure 2G), confirming increased NAD levels compared with GFP control cells ($P < .001$) (Figure 2H). NAMPT-infected cells acquired resistance to chronic exposure to BRAFi earlier than their GFP-infected counterparts (Figure 2I) and showed a more aggressive behavior than control cells in terms of growth ($P < .001$) and wound-repairing properties ($P < .001$) (Figure 2J).

Transcriptional Regulation of NAMPT in MM Cells

Because NAMPT transcription is regulated by inflammatory stress signals (29–31), we hypothesized a direct link between *NAMPT* transcription and BRAF signaling. In line with this hypothesis, the MEK inhibitor pimasertib, alone or in combination with dabrafenib, statistically significantly impaired NAMPT expression in BiR cells. Dabrafenib reduced *NAMPT* transcription selectively in S, but not in BiR cells (Figure 3A). These effects were also evident at the protein level, as shown by confocal microscopy (Figure 3B). NAD quantification in treated cells confirmed that inhibition of MAPK signaling decreased NAD levels (mean NAD levels in untreated [UN] M14/BiR = 9.8 ±.1.4 vs 3.7 ±30.6 nmol/mg in cells treated with BRAFi+MEKi [C], $P = .001$; mean in UN A375/BiR cells = 6.4 ± 0.7 vs 1.4 ± 0.1 nmol/mg in treated cells, $P < .001$) (Figure 3C).

We then asked how NAMPT expression is regulated in BiR cells. M14 showed a constitutively active HIF-1α pathway, as demonstrated by the finding of a predominantly nuclear HIF-1α, as opposed to M14/S cells where it was mostly cytoplasmic. *HIF1A* expression levels were also slightly increased in M14/BiR vs M14/S cells ($P = .03$) (Figure 4A). A375/BiR cells, on the contrary, showed constitutive STAT3 phosphorylation at tyr705, at variance with A375/S cells (Figure 4B; Supplementary Figure 4A, available online). The finding of increased mRNA levels of microphthalmia-associated transcription factor (*MITF*) (Figure 4C), selectively in A375/BiR cells ($P = .001$ BiR vs S cells), substantiated activation of STAT3 transcriptional program and was in line with the documented upregulation of PGC-1α expression (32–34) (Figure 1I). Furthermore, A375/BiR cells showed constitutive phosphorylation and nuclear translocation of the p65 subunit of the NF-kB complex (Figure 4D; Supplementary Figure 4B, available online), which modulates mitochondrial respiration through cytochrome C oxidase assembly protein 2 (*SCO2*) (35), overexpressed in A375/BiR cells ($P = .02$ in BiR vs S cells) (Figure 4E).

Chromatin immunoprecipitation (ChIP) experiments showed that NF-kB and STAT3 bind to the *NAMPT* promoter in A375/BiR cells, while HIF-1α binds in M14/BiR cells (Figure 4F), confirming that both OXPHOS and glycolysis converge on NAMPT as a common transcriptional target.

NAMPT Expression in Tissue Biopsies from BRAF-Mutated Melanoma Patients Before and After the Acquisition of Resistance to BRAFi

We then analyzed NAMPT expression in tissue biopsies from patients with MM obtained for diagnostic purposes, documenting marked NAMPT upregulation in melanoma lesions compared with normal melanocytes (Figure 5A). NAMPT expression was then measured in biopsies from 17 MM patients obtained before and after development of resistance to BRAFi. Robust NAMPT upregulation in BiR samples was highlighted in 14 of 17 patients, with highly statistically significant differences when combining NAMPT intensity and score (mean NAMPT score before BRAFi treatment [S] = 106.5 ± 69.3 vs 210.3 ± 81.2 in BiR tissues, $P < .001$) (Figure 5B). NAMPT staining in a representative patient is shown in Figure 5C.

Expression of the other three NBEs was either decreased or unchanged, showing that NAMPT is the dominant NBE in these lesions, indirectly validating our cell lines (Figure 5D).

Figure 4. Continued

The **small squares** in **(A)**, **(B)**, and **(D)** represent the zoomed area defined by the **white perimeter**. **F)** Schematic representation of *NAMPT* gene promoter and its regulatory elements with consensus binding sequences for the indicated transcription factors. Specific primers N1, N2, and N3 were used in chromatin immunoprecipitation experiments (**upper panel**). Semiquantitative PCR analysis of the *NAMPT* promoter, highlighted with the indicated primers in total chromatin preparations (INPUT) and after immunoprecipitation with isotypic control (ISO) or with antibodies recognizing STAT3 and NF-kB for A375/BiR and HIF-1α for M14/BiR cells (**bottom panel**). Box plots on the **right** show cumulative data obtained from four independent experiments. The relative STAT3-NF-kB (for A375/BiR cells) and HIF-1α (for M14/BiR cells) binding affinity for *NAMPT* promoter was calculated as the ratio between the intensity of the band amplified after immunoprecipitation (either with the specific antibody or the ISO) and the band amplified in the input DNA. Results are represented as percentage of input. All statistical analyses were performed using two-sided Mann–Whitney U test. **Boxes** represent interquartile range, and the **horizontal line across each box** indicates the median. BiR = BRAFi-resistant; ChIP = chromatin immunoprecipitation; ISO = isotypic control; NAMPT = nicotinamide phosphoribosyltransferase; S = BRAFi-sensitive.

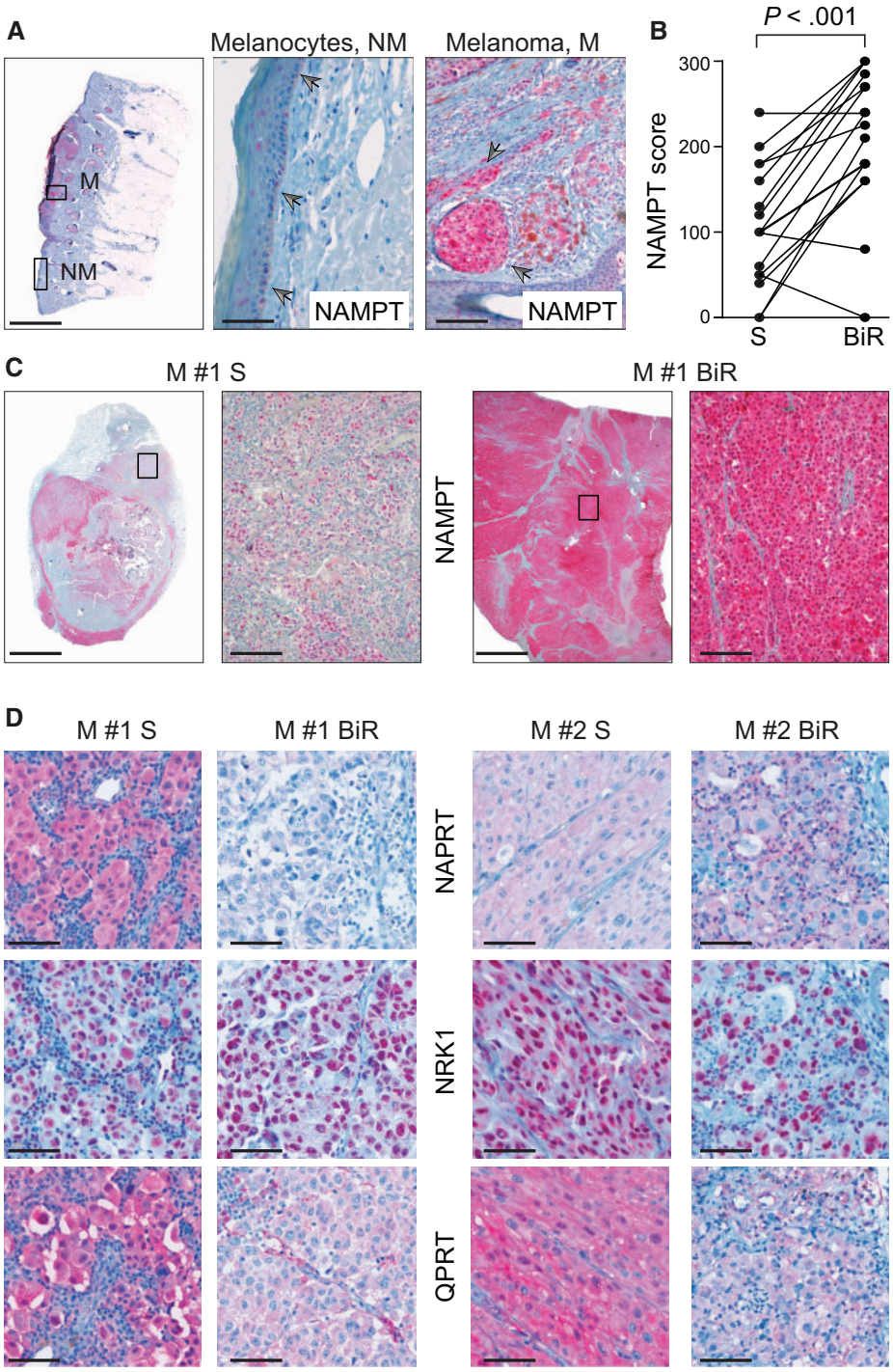

Figure 5. Nicotinamide phosphoribosyltransferase (NAMPT) expression in tissues from metastic melanoma (MM) patients before and after developing resistance to BRAFi. **A)** Immunohistochemical staining with NAMPT in a skin biopsy from a patient with melanoma. Areas with normal melanocytes (NM; **arrows in the middle panel**) or with melanoma (M; **arrows in the right panel**) are shown. Original magnification 2.5 × (**left image**). **Scale bar** = 800 μm and 20×, **scale bar** = 100 μm. **B)** NAMPT expression was evaluated using an ad hoc devised score that considered both the percentage of positive cells and their intensity in paired biopsies from 17 patients obtained before and after the onset of resistance to BRAFi. Statistical analysis was performed using two-sided Wilcoxon tests. **C)** The images show the result of an immunohistochemical analysis of NAMPT expression in a biopsy from a patient with MM before treatment with BRAFi (**left panel**, S) and after the patient became resistant to therapy (**right panel**, BiR). The insets show 2.5 magnification, while the panels have an original magnification of 20×. **Scale bar** = 100 μm. **D)** Immunohistochemical analysis of NAPRT/NRK/QPRT expression in biopsies from two patients with metastatic melanoma before treatment with BRAFi (S) and after the patients became resistant to therapy (BiR). Original magnification 40×. **Scale bar** = 50 μm. BiR = BRAFi-resistant; M = melanoma; NAMPT = nicotinamide phosphoribosyltransferase; NM = melanocyte; S = BRAFi-sensitive; UN = untreated.

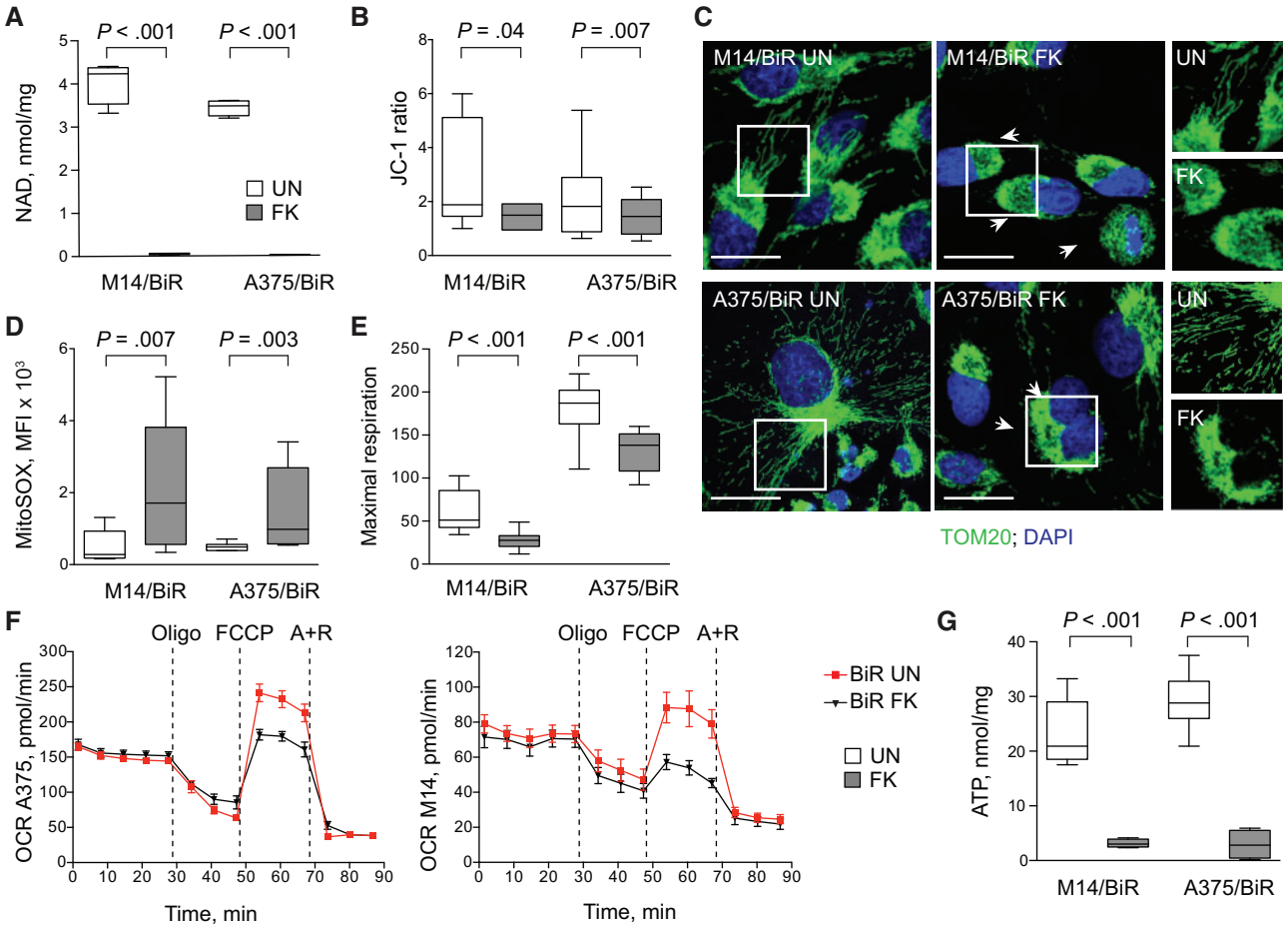

Figure 6. Effects of nicotinamide phosphoribosyltransferase (NAMPT) inhibition on mitochondrial functions. **A)** Intracellular NAD levels were measured in BRAFi-sensitive (s) or -resistant (BiR) cells after treatment with FK866 (25 nM, 72 hours). Results are expressed as nmol/mg proteins and are derived from four independent experiments. **B)** Box plot showing mitochondrial membrane potential after treatment with FK866 (25 nM), as measured after staining with JC-1. Results are expressed as the ratio between red and green fluorescence. The shift from red to green (ie, a decrease in the ratio) indicates mitochondrial membrane depolarization. **C)** Confocal microscopy images show staining with anti-TOM20 antibody (a mitochondrial marker) in BiR cells treated with FK866 (25 nM, 48 hours). **Arrows** in the FK-treated panels indicate swelled mitochondria. The **small squares** represent the zoomed area defined by the **white perimeter**. Nuclei were counterstained with DAPI. Original magnification 63×. **Scale bar** = 25 μm. **D) Box plot on the left** shows mean fluorescence intensity values of BiR cells treated with FK866 (25 nM, 48 hours) and stained with MitoSOX, a mitochondrial ROS-specific probe. **E)** Cumulative data showing maximal respiration values calculated as: (oxygen consumption rate [OCR] after FCCP injection – OCR after antimycin+rotenone addition). **F)** Representative OCR plots for S and BiR cells cultured with FK866 (25 nM, 18 hours). **G)** Box plot showing intracellular ATP concentrations (nmol/mg proteins) in S or BiR cells treated with FK866 (25 nM, 72 hours). Cumulative results from four independent experiments. All statistical analyses were performed using two-sided Wilcoxon or paired *t* tests. **Boxes** represent interquartile range, and the **horizontal line across each box** indicates the median. A+R = antimycin+rotenone; BiR = BRAFi-resistant; FCCP = carbonyl cyanide p-trifluoromethoxyphenylhydrazone; Oligo = oligomycin; S = BRAFi-sensitive.

Effects of NAMPT Inhibition on Mitochondrial Functions

These data provide rationale to the use of NAMPTi in the therapy of BiR melanomas. We therefore tested the effects of FK866 and GMX1778 in M14/BiR and A375/BiR variants.

Exposure to FK866 caused a drastic reduction in NAD levels, which became undetectable after 72 hours ($P < .001$ in untreated vs FK866-treated [FK] cells) (Figure 6A). This effect was evident starting at 5 nM FK866 in A375/BiR and at 10 nM in M14/BiR cells, in line with higher NAMPT levels in the latter cells (Supplementary Figure 5A, available online). However, as NAD was undetectable in both cell lines at 25 nM FK866, this dose was adopted in further experiments.

NAD depletion by FK866 was followed (18–24 hours) by the depolarization of the inner mitochondrial membrane (IMM) with loss of mitochondrial membrane potential ($\Delta\psi m$, $P = .04$ and $P = .007$ UN vs FK for M14/BiR and A375/BiR, respectively) (Figure 6B). Mitochondria of FK866-treated cells were swelled and fragmented, as indicated by TOM20 staining (Figure 6C). The effect of FK866 on mitochondrial morphology was particularly evident in A375/BiR, which rely mostly on OXPHOS and display a highly developed mitochondrial network. As expected (36), depolarization of the IMM triggered ROS release (Figure 6D) and drastically decreased maximal respiratory capacity of FK866-treated cells ($P < .001$ UN vs FK) (Figure 6E). However, while exposure to FK866 (18 hours) did not reduce steady-state OCR or response to oligomycin, it decreased responses to the uncoupler FCCP, suggesting that NAMPTi affects bioenergetic efficiency (Figure 6F). Consequently, ATP levels in FK866-treated cells dropped dramatically and in a dose-dependent way compared with control cells ($P < .001$ UN vs FK) (Figure 6G; Supplementary Figure 5B, available online). These data suggest that FK866 damages mitochondria and limits the cellular metabolic capacity.

ARTICLE

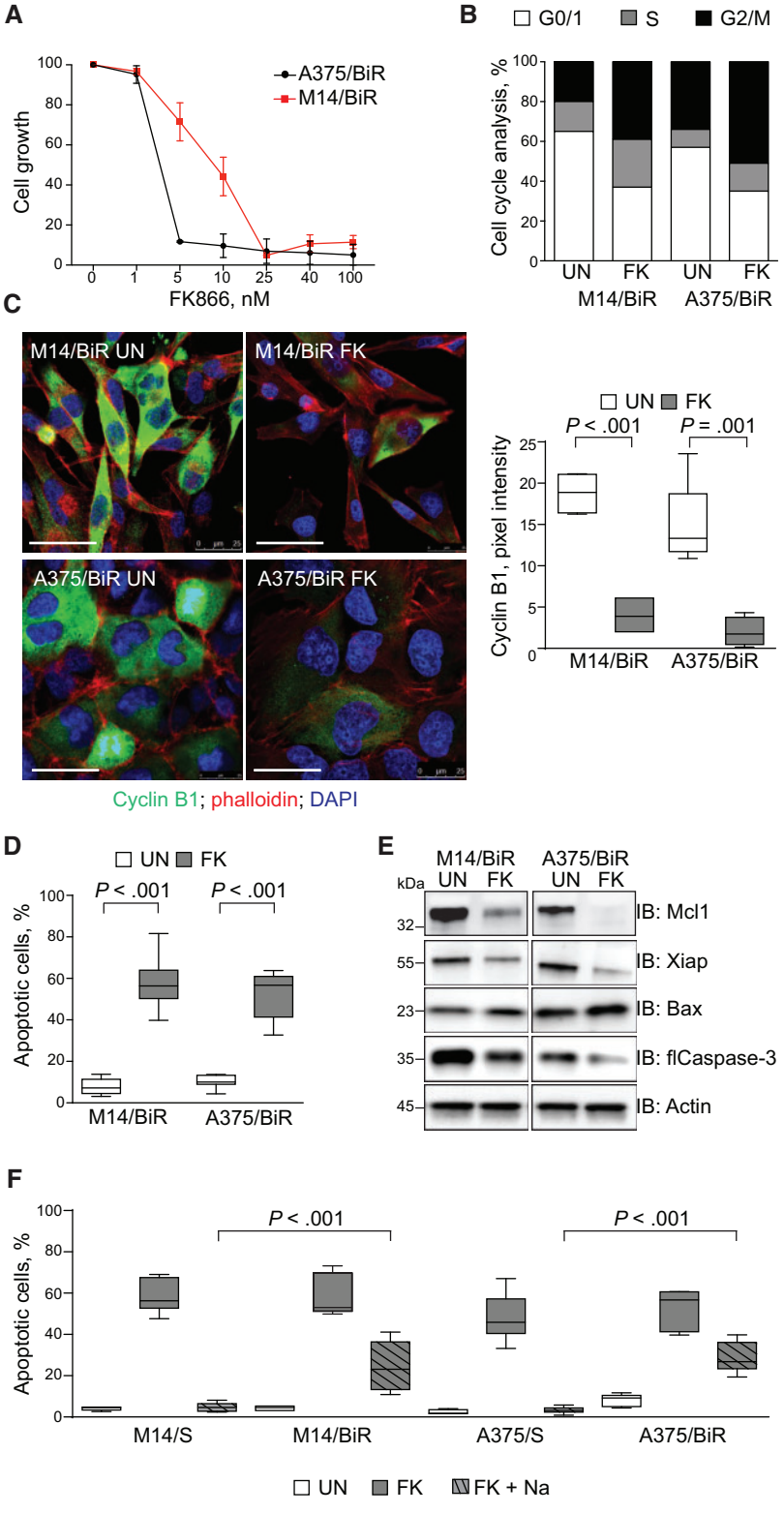

Figure 7. Effects of nicotinamide phosphoribosyltransferase (NAMPT) inhibition on melanoma cell growth and apoptosis. **A)** Results from MTT assays performed using BRAFi-sensitive (s) or -resistant (BiR) cells treated for 72 hours with different concentrations of FK866. Data are represented as percentage of control (untreated cells). **B)** Cell cycle distribution of S or BiR cells treated with FK866 (25 nM, 48 hours) determined by flow cytometry analysis. At least six independent experiments were performed. **C)** Confocal microscopy showing cyclin B1 expression in BiR cells treated with FK866 (25 nM for 48 hours). Cells were counterstained with phalloidin and DAPI to highlight the cytoplasm and the nucleus. Original magnification 63×. **Scale bar** = 25 μm. Box plot on the **right** shows the quantification of cyclin B1 fluorescence (pixel intensity) in at least five independent experiments. Statistical analysis was performed using two-sided Wilcoxon test. **D)** Box plot showing the percentage of cells undergoing apoptosis in the presence of FK866 (25 nM, 72 hours). Positive cells included AnnexinV$^+$, PI$^+$, and double-positive cells. At least eight independent experiments were performed. Statistical analysis was performed using two-sided Wilcoxon test. **E)** Representative immunoblot using lysates of BiR cells treated with FK866 (25 nM, 48 hours). Actin was added as loading control. **F)** Box plots showing percentage of apoptosis in S and BiR cells treated with FK866 for 72 hours with or without nicotinic acid (Na, 0.2 μM), added at the beginning of the culture. Results from five independent experiments. Statistical analysis was performed using two-sided Mann–Whitney U test. All **boxes** represent interquartile range, and the **horizontal line across each box** indicates median value. BiR = BRAFi-resistant; flCaspase3 = full-length caspase 3; S = BRAFi-sensitive.

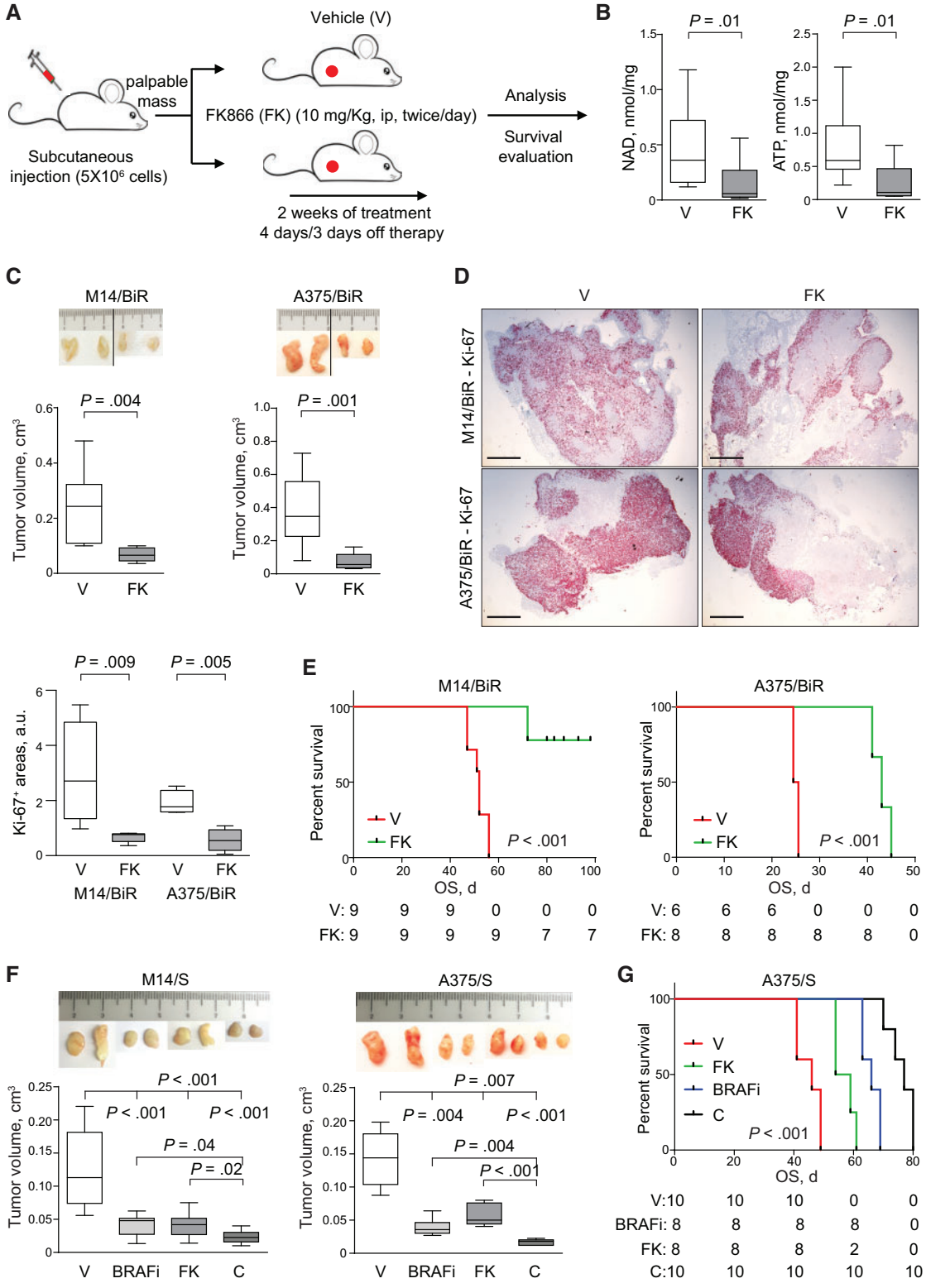

Figure 8. Effects of nicotinamide phosphoribosyltransferase (NAMPT) inhibition in melanoma xenografts. **A)** NOD/SCID/γchain$^{-/-}$ (NSG) mice (n = 6–10 mice per group) were injected subcutaneously with A375/BRAFi-resistant (BiR) and M14/BiR cells. When tumors became palpable, mice xenografted with BiR cells were treated with FK866 as a single drug. Treatment was repeated for four consecutive days, followed by three days off therapy in a two-week cycle. Assessment of tumor was performed after the end of the second week of treatment. A second set of mice was followed for survival studies. **B)** Box plots showing intracellular NAD and ATP concentrations in BiR cells xenografted in NSG mice and treated with vehicles (V) and FK866 (FK) for the two-week schedule described in **(A)**. **C)** Box plots showing tumor volumes of BiR cells xenografted in NSG mice and treated as indicated. Representative images of tumor masses are shown. **D)** Representative images of Ki-67 staining in BiR cells treated as indicated. Original magnification 2.5×. **Scale bar** = 800 μm. Box plot showing Ki-67-positive areas in indicated cells and treatments. At least six samples were quantified. All statistical analyses were performed using two-sided Mann–Whitney U test. **Boxes** represent interquartile range, and the **horizontal line across each box** indicates the median. **E)** Kaplan-Meier curves showing survival of mice xenografted with BiR cells and treated for two weeks with FK866 as a single drug. The P value

Effects of NAMPT Inhibition on Cell Growth and Apoptosis

Culture of A375/BiR and M14/BiR cells with FK866 or GMX1778 for 72 hours blocked cell growth (Figure 7A; Supplementary Figure 6A, available online). However, analysis of the cell cycle after 48 hours of FK866 exposure showed accumulation of cells in the S and G2/M phases (Figure 7B; Supplementary Figure 6B, available online), suggesting that FK866 causes G2/M cell cycle arrest. G2/M transition is regulated by cyclin B1/Cdk1 (37–39), which was markedly decreased after a 48-hour culture with FK866 ($P < .001$ and $P = .001$ UN vs FK for M14/BiR and A375/BiR, respectively) (Figure 7C).

Staining with annexin V and propidium iodide after 72 hours of culture with FK866 or GMX1778 confirmed induction of apoptosis ($P < .001$ in both BiR variants) (Figure 7D; Supplementary Figure 6, C and D, available online), with downregulation of the prosurvival molecules Mcl-1 and Xiap, upregulation of the proapoptotic protein Bax, and caspase3 activation (Figure 7E). In line with the hypothesis that NAMPT is the dominant NBE in BiR cells, extracellular supplementation of nicotinic acid (Na, the substrate for the NAPRT-regulated pathway) completely rescued from FK866-induced apoptosis, at variance with S cells, where apoptosis was completely inhibited ($P < .001$ FK +Na in S cells vs FK + Na in BiR cells in both cell lines) (Figure 7F).

Effects of NAMPTi in Xenograft Models of BiR Melanomas

To assess the therapeutic potential of NAMPTi, A375/BiR and M14/BiR cells were xenografted into NSG mice (n = 6–10 /group). When tumors became palpable, mice were randomly assigned to receive vehicle or FK866 (Figure 8A). As expected, BiR tumors obtained from FK866-treated mice contained less NAD and ATP when compared with tumors treated with the vehicle (V) only ($P = .01$) (Figure 8B). Marked and statistically significant reduction in tumor volume and weight, as well as in proliferating cells, with a parallel increase in necrotic areas, was recorded in the FK866-treated mice, without apparent signs of toxicity (Figure 8, C and D; Supplementary Figure 7, A and B, available online).

When monitoring mice after treatment, we noticed that FK866 markedly prolonged survival of mice xenografted with M14/BiR and A375/BiR. In A375/BiR-injected mice, median survival of vehicle-treated mice was 23.5 days vs 43 days for FK866-treated ones ($P < .001$) (Figure 8E). In M14/BiR xenografts, vehicle-treated mice showed a median survival of 52 days, while mice treated with FK866 did not reach a median survival at 100 days, when all live mice (seven of nine in the FK866 arm) were killed ($P < .001$) (Figure 8E). Of these, five had no evidence of disease but displayed infiltration of murine myeloid cells at the site of injection.

When the same experiment was performed on M14/S and A375/S cells, maximal and statistically significant responses in terms of decrease in tumor volume and weight and increase in necrotic areas were obtained by combining FK866 and BRAFi (Figure 8F; Supplementary Figure 7, C and D, available online). Survival analysis performed in A375/S cells confirmed that the combination of FK866 and BRAFi yielded the best results in terms of mouse survival: median survival of vehicle-treated mice was 46 days vs 77 days for FK866/BRAFi combination-treated mice ($P < .001$) (Figure 8G). On the contrary, median survival of FK866-treated mice was only 56.5, and in BRAFi-treated mice it was only 66 ($P < .001$) (Figure 8G). These data suggest that the combination of BRAFi and NAMPTi should be further explored as new therapeutic possibility in BRAFi-sensitive patients.

Discussion

To study NAD metabolism in different phases of tumor transformation, we selected two BRAF-mutated melanoma cell lines (M14 and A375) that were made resistant to BRAFi by chronic exposure to dabrafenib. Resistant cells showed paradoxical overactivation of the MAP kinase pathway downstream of BRAF and increased aerobic glycolysis or OXPHOS in M14 and A375, respectively. This different metabolic adaptation was regulated through the activation of transcription factors that control expression of glycolytic or mitochondrial metabolic genes. In line with a Warburg phenotype, resistance to BRAFi in M14 cells stabilized HIF-1α, with upregulation of HK2 and of LDHA, two critical enzymes in glucose metabolism. On the contrary, A375/BiR cells showed constitutive NF-KB and STAT3 signaling, with activation of MITF transcription factor and PGC-1α, which enhances expression and activity of the ATP synthase. Interestingly, these two pathways appear mutually exclusive, suggesting that therapeutic targeting may be broadly effective only if a common element is selected.

Our findings show that in both cell lines and independent of the preferred metabolic pathway, NAD levels increase when cells become resistant to BRAFi, and the NAD biosynthetic pathway that uses nicotinamide becomes the dominant one. In this pathway, nicotinamide is transformed into nicotinamide mononucleotide (NMN) through the rate-limiting activity of NAMPT, and it is subsequently converted to NAD by NMNATs, which exist in three isoforms and which are abundantly present in different cell districts, including mitochondria. Our data indicate that in both BiR cell lines NAMPT is upregulated, while the other rate-limiting NBEs in NAD metabolism are not modulated. The findings that cell lines overexpressing NAMPT develop earlier resistance to BRAFi, grow faster, and repair wounds more efficiently suggest that NAMPT is directly involved in determining the disease aggressiveness of BRAF-mutated melanomas. Accordingly, inhibition of MAPK signaling decreased NAD levels in both S and BiR cells. Furthermore, analysis of tissue biopsies of patients obtained before and after resistance to BRAFi confirmed NAMPT induction in the BiR state. NAMPT overexpression was regulated by NF-kB, STAT3, and HIF-1α, the same transcription factors that regulate OXPHOS and glycolysis.

These results suggest that BiR cells are uniquely sensitive to NAMPT targeting. By using two validated NAMPTi, FK866 and GMX1778, we observed a dramatic drop in cellular NAD levels

Figure 8. Continued
was calculated using log-rank test. Nine mice per condition for M14/BiR and at least six for A375/BiR cells were studied. **F)** Box plot showing tumor volumes of M14/BRAFi-sensitive (S) and A375/S cells xenografted in NSG mice and treated as indicated: V, BRAFi, FK, and FK866/BRAFi combination (C). Representative images of tumor masses are shown. Statistical analysis was performed using two-sided multiple comparisons or Mann–Whitney U tests. **Boxes** represent interquartile range, and the **horizontal line across each box** indicates the median. **G)** Kaplan-Meier curves showing survival of mice xenografted with A375/S cells and treated for two weeks as indicated ($P < .001$ in all the treatment conditions compared with V, log-rank test; n = 10 mice for V and C, n = 8 mice for single-agent FK and BRAFi). a.u. = arbitrary unit; BiR = BRAFi-resistant; C = combination; OS = overall survival; S = BRAFi-sensitive; V = vehicle.

following exposure to both drugs, confirming that the Nam-dependent pathway is the primary route to generate NAD in these cells. In line with this hypothesis, supplementation of BiR cells with artificially high levels of extracellular Na (in order to maximize activity of the NAPRT-controlled pathway) failed to completely rescue BiR cells from FK866-mediated apoptosis, at variance with what was observed with S cells. NAD depletion in BiR cells disrupted mitochondrial energy production, causing swelling and loss of membrane potential, with ROS accumulation. Cells were blocked in the G2/M phase of the cell cycle and underwent activation of mitochondrial-dependent cell death. These data are in line with recent findings, which connect mitochondrial respiration to cell cycle progression, especially in the G2/M transition, which is an energy-sensitive checkpoint. Reportedly, cyclin B1/Cdk1, the checkpoint kinase for the G2→M transition, increases mitochondrial respiration, enhancing oxygen consumption and ATP generation (40). Therefore, the strong decrease in cyclin B1 expression observed after FK866 treatment could impact OXPHOS, linking G2/M block to mitochondrial dysfunction. The therapeutic potential of NAMPTi was then validated using xenograft models. Both A375/BiR and M14/BiR cell lines responded well to FK866 administered as a single agent, showing a statistically significant decrease of tumor growth and marked extension of survival. Importantly, five of nine mice xenografted with M14/BiR cells were disease free after 100 days following two weeks treatment with NAMPTi. Interestingly, while S cells were less sensitive to FK866 used as a single agent, as expected, its combination with a BRAFi yielded the best effects in terms of tumor growth and mouse survival, suggesting that this therapeutic avenue should be further investigated. Importantly, no signs of toxicity were observed in these mice, in line with the idea that normal cells use multiple pathways to synthesize NAD, at variance with BiR cells, which appear to rely predominantly on NAMPT.

A potential limitation of the study concerns the identification of the patients that will benefit the most from therapy with NAMPTi, either alone or in combination with BRAFi. We are currently testing the hypothesis that plasmatic concentrations of NAMPT may actually reflect intracellular ones, as shown in other models (41). A second issue that needs to be investigated further is the role of eNAMPT in shaping the tumor microenvironment: immunocompetent mouse models of melanoma, together with patient studies, will be useful to the purpose.

In conclusion, our results show that NAMPT is an actionable target for selected subsets BRAF-mutated melanoma patients.

Funding

This work was supported by the Italian Institute for Genomic Medicine (formerly HuGeF) Institutional funds, by University of Torino and Polytechnic University of Marche research grants, by the Associazione Italiana per la Ricerca sul Cancro AIRC (IG-17314 to SD), and by Fondazione Ente Cassa di Risparmio di Firenze (2014.0240 to DM). VA was supported by FIRC/AIRC triennial (#15047) and "Carlo Chianello" Foundation fellowships and is now supported by "Franco e Marilisa Caligara" Foundation fellowships.

Notes

The funders had no role in the design of the study; the collection, analysis, or interpretation of the data; the writing of the manuscript; or the decision to submit the manuscript for publication. The other authors declare no competing financial interests.

Thanks are given to Katiuscia Gizzi for excellent technical support. The authors also wish to acknowledge the help of Prof. Giuseppe Matarese and Dr. Claudio Procaccini (Lab of Immunology, Istituto di Endocrinologia e Oncologia Sperimentale, Consiglio Nazionale delle Ricerche [IEOS-CNR], University of Naples "Federico II," Naples, Italy) for training VA to use the Seahorse technology. TOM20 antibody was a kind gift from Prof. Ildikò Szabò (University of Padua, Padua, Italy).

Author contributions: VA designed and performed experiments and wrote the paper; AM, SLV, FZ, NV, GB, SC, SS, CB, AS, FA, and TV performed experiments; MM provided patient samples; DM, MM, and NR interpreted data; SD designed experiments, interpreted data, and wrote the paper.

References

1. Cairns RA, Harris IS, Mak TW. Regulation of cancer cell metabolism. *Nat Rev Cancer*. 2011;11(2):85–95.
2. Chiarugi A, Dolle C, Felici R, et al. The NAD metabolome—a key determinant of cancer cell biology. *Nat Rev Cancer*. 2012;12(11):741–752.
3. Verdin E. NAD(+) in aging, metabolism, and neurodegeneration. *Science*. 2015; 350(6265):1208–1213.
4. Burgos ES. NAMPT in regulated NAD biosynthesis and its pivotal role in human metabolism. *Curr Med Chem*. 2011;18(13):1947–1961.
5. Garten A, Schuster S, Penke M, et al. Physiological and pathophysiological roles of NAMPT and NAD metabolism. *Nat Rev Endocrinol*. 2015;11(9):535–546.
6. Wachsman W, Morhenn V, Palmer T, et al. Noninvasive genomic detection of melanoma. *Br J Dermatol*. 2011;164(4):797–806.
7. Maldi E, Travelli C, Caldarelli A, et al. Nicotinamide phosphoribosyltransferase (NAMPT) is over-expressed in melanoma lesions. *Pigment Cell Melanoma Res*. 2013;26(1):144–146.
8. Galli U, Travelli C, Massarotti A, et al. Medicinal chemistry of nicotinamide phosphoribosyltransferase (NAMPT) inhibitors. *J Med Chem*. 2013;56(16): 6279–6296.
9. Montecucco F, Cea M, Bauer I, et al. Nicotinamide phosphoribosyltransferase (NAMPT) inhibitors as therapeutics: Rationales, controversies, clinical experience. *Curr Drug Targets*. 2013;14(6):637–643.
10. Sampath D, Zabka TS, Misner DL, et al. Inhibition of nicotinamide phosphoribosyltransferase (NAMPT) as a therapeutic strategy in cancer. *Pharmacol Ther*. 2015;151:16–31.
11. Tan B, Young DA, Lu ZH, et al. Pharmacological inhibition of nicotinamide phosphoribosyltransferase (NAMPT), an enzyme essential for NAD+ biosynthesis, in human cancer cells: Metabolic basis and potential clinical implications. *J Biol Chem*. 2013;288(5):3500–3511.
12. Davies H, Bignell GR, Cox C, et al. Mutations of the BRAF gene in human cancer. *Nature*. 2002;417(6892):949–954.
13. Flaherty KT, Puzanov I, Kim KB, et al. Inhibition of mutated, activated BRAF in metastatic melanoma. *N Engl J Med*. 2010;363(9):809–819.
14. Chapman PB, Hauschild A, Robert C, et al. Improved survival with vemurafenib in melanoma with BRAF V600E mutation. *N Engl J Med*. 2011;364(26): 2507–2516.
15. Hauschild A, Grob JJ, Demidov LV, et al. Dabrafenib in BRAF-mutated metastatic melanoma: A multicentre, open-label, phase 3 randomised controlled trial. *Lancet*. 2012;380(9839):358–365.
16. Garraway LA, Janne PA. Circumventing cancer drug resistance in the era of personalized medicine. *Cancer Discov*. 2012;2(3):214–226.
17. Flaherty KT, Infante JR, Daud A, et al. Combined BRAF and MEK inhibition in melanoma with BRAF V600 mutations. *N Engl J Med*. 2012;367(18):1694–1703.
18. Parmenter TJ, Kleinschmidt M, Kinross KM, et al. Response of BRAF-mutant melanoma to BRAF inhibition is mediated by a network of transcriptional regulators of glycolysis. *Cancer Discov*. 2014;4(4):423–433.
19. Abildgaard C, Guldberg P. Molecular drivers of cellular metabolic reprogramming in melanoma. *Trends Mol Med*. 2015;21(3):164–171.
20. Smith LK, Rao AD, McArthur GA. Targeting metabolic reprogramming as a potential therapeutic strategy in melanoma. *Pharmacol Res*. 2016;107:42–47.
21. Ratnikov BI, Scott DA, Osterman AL, et al. Metabolic rewiring in melanoma. *Oncogene*. 2017;36(2):147–157.
22. Mori V, Amici A, Mazzola F, et al. Metabolic profiling of alternative NAD biosynthetic routes in mouse tissues. *PLoS One*. 2014;9(11):e113939.
23. Pollock PM, Harper UL, Hansen KS, et al. High frequency of BRAF mutations in nevi. *Nat Genet*. 2003;33(1):19–20.
24. Haq R, Shoag J, Andreu-Perez P, et al. Oncogenic BRAF regulates oxidative metabolism via PGC1alpha and MITF. *Cancer Cell*. 2013;23(3):302–315.
25. Vazquez F, Lim JH, Chim H, et al. PGC1alpha expression defines a subset of human melanoma tumors with increased mitochondrial capacity and resistance to oxidative stress. *Cancer Cell*. 2013;23(3):287–301.

26. Bettum IJ, Gorad SS, Barkovskaya A, et al. Metabolic reprogramming supports the invasive phenotype in malignant melanoma. *Cancer Lett*. 2015;366(1):71–83.
27. Ruggieri S, Orsomando G, Sorci L, et al. Regulation of NAD biosynthetic enzymes modulates NAD-sensing processes to shape mammalian cell physiology under varying biological cues. *Biochim Biophys Acta*. 2015;1854(9):1138–1149.
28. Zamporlini F, Ruggieri S, Mazzola F, et al. Novel assay for simultaneous measurement of pyridine mononucleotides synthesizing activities allows dissection of the NAD(+) biosynthetic machinery in mammalian cells. *FEBS J*. 2014;281(22):5104–5119.
29. Ognjanovic S, Bao S, Yamamoto SY, et al. Genomic organization of the gene coding for human pre-B-cell colony enhancing factor and expression in human fetal membranes. *J Mol Endocrinol*. 2001;26(2):107–117.
30. Nowell MA, Richards PJ, Fielding CA, et al. Regulation of pre-B cell colony-enhancing factor by STAT-3-dependent interleukin-6 trans-signaling: Implications in the pathogenesis of rheumatoid arthritis. *Arthritis Rheum*. 2006;54(7):2084–2095.
31. Romacho T, Azcutia V, Vazquez-Bella M, et al. Extracellular PBEF/NAMPT/visfatin activates pro-inflammatory signalling in human vascular smooth muscle cells through nicotinamide phosphoribosyltransferase activity. *Diabetologia*. 2009;52(11):2455–2463.
32. Levy C, Khaled M, Fisher DE. MITF: Master regulator of melanocyte development and melanoma oncogene. *Trends Mol Med*. 2006;12(9):406–414.
33. Hartman ML, Czyz M. MITF in melanoma: Mechanisms behind its expression and activity. *Cell Mol Life Sci*. 2015;72(7):1249–1260.
34. Wan P, Hu Y, He L. Regulation of melanocyte pivotal transcription factor MITF by some other transcription factors. *Mol Cell Biochem*. 2011;354(1–2):241–246.
35. Mauro C, Leow SC, Anso E, et al. NF-kappaB controls energy homeostasis and metabolic adaptation by upregulating mitochondrial respiration. *Nat Cell Biol*. 2011;13(10):1272–1279.
36. Murphy MP. How mitochondria produce reactive oxygen species. *Biochem J*. 2009;417(1):1–13.
37. Gavet O, Pines J. Progressive activation of CyclinB1-Cdk1 coordinates entry to mitosis. *Dev Cell*. 2010;18(4):533–543.
38. Yuan J, Yan R, Kramer A, et al. Cyclin B1 depletion inhibits proliferation and induces apoptosis in human tumor cells. *Oncogene*. 2004;23(34):5843–5852.
39. Liu Q, Tao B, Liu G, et al. Thromboxane A2 receptor inhibition suppresses multiple myeloma cell proliferation by inducing p38/c-jun N-terminal kinase (JNK) mitogen-activated protein kinase (MAPK)-mediated G2/M progression delay and cell apoptosis. *J Biol Chem*. 2016;291(9):4779–4792.
40. Wang Z, Fan M, Candas D, et al. Cyclin B1/Cdk1 coordinates mitochondrial respiration for cell-cycle G2/M progression. *Dev Cell*. 2014;29(2):217–232.
41. Audrito V, Serra S, Brusa D, et al. Extracellular nicotinamide phosphoribosyltransferase (NAMPT) promotes M2 macrophage polarization in chronic lymphocytic leukemia. *Blood*. 2015;125(1):111–123.